Monthly Notices
of the
ROYAL ASTRONOMICAL SOCIETY

MNRAS **483,** 1256–1264 (2019)
Advance Access publication 2018 November 27

doi:10.1093/mnras/sty3205

The infrared-luminous progenitors of high-z quasars

M. Ginolfi,[1,2★] R. Schneider,[2,3] R. Valiante,[1] E. Pezzulli,[2,3] L. Graziani,[2,4] S. Fujimoto[5] and R. Maiolino[6,7]

[1]*INAF/Osservatorio Astronomico di Roma, Via di Frascati 33, I-00040 Monte Porzio Catone, Italy*
[2]*Dipartimento di Fisica, Sapienza Università di Roma, Piazzale Aldo Moro 5, I-00185 Roma, Italy*
[3]*INFN, Sezione di Roma I, P.le Aldo Moro 2, I-00185 Roma, Italy*
[4]*Scuola Normale Superiore, piazza dei Cavalieri, 7, I-56126 Pisa, Italy*
[5]*Institute for Cosmic Ray Research, The University of Tokyo, Kashiwa, Chiba 277-8582, Japan*
[6]*Cavendish Laboratory, University of Cambridge, 19 J.J. Thomson Ave., Cambridge CB3 0HE, UK*
[7]*Kavli Institute for Cosmology, University of Cambridge, Madingley Road, Cambridge CB3 0HA, UK*

Accepted 2018 November 20. Received 2018 November 2; in original form 2018 September 22

ABSTRACT

Here we explore the infrared (IR) properties of the progenitors of high-z quasar host galaxies. Adopting the cosmological, data-constrained semi-analytic model GAMETE/QSOdust, we simulate several independent merger histories of a luminous quasar at $z \sim 6$, following black hole growth and baryonic evolution in all its progenitor galaxies. We find that a fraction of progenitor galaxies (about 0.4 objects per single luminous quasar) at $6.5 < z < 8$ has an IR luminosity of $L_{\rm IR} > 10^{13}\,{\rm L}_{\odot}$ (hyper-luminous IR galaxies; HyLIRGs). HyLIRGs progenitors reside in the most massive haloes, with dark matter (DM) masses of $M_{\rm DM} \sim 10^{12.5}$–$10^{13}\,{\rm M}_{\odot}$. These systems can be easily observed in their $\sim$1 mm-continuum emission in a few seconds of integration time with the Atacama Large Millimeter/submillimeter Array, and at least 40 per cent of them host nuclear black hole activity that is potentially observable in the soft and hard X-ray band. Our findings are in line with recent observations of exceptional massive DM haloes hosting HyLIRGs at $z \sim 7$, suggesting that $z \sim 6$ luminous quasars are indeed the signposts of these observed rare peaks in the high-z cosmic density field, and that massive IR-luminous galaxies at higher z are their natural ancestors.

Key words: galaxies: evolution – galaxies: high-redshift – quasars: general – infrared: galaxies – submillimetre: galaxies.

1 INTRODUCTION

Observations of dusty star-forming galaxies (DSFGs) at high-redshift, often selected at (sub-)millimeter wavelengths (submillimeter galaxies, or SMGs; Smail, Ivison & Blain 1997; Hughes et al. 1998; Chapman et al. 2005; Hayward et al. 2013), can provide unique insights into our understanding of the early formation of massive galaxies (see e.g. Blain et al. 2002; Casey, Narayanan & Cooray 2014 for reviews). Because of their large dust content, DSFGs emit most of their luminosity at infrared (IR) wavelengths (8–1000 μm) and are typically considered ultraluminous IR galaxies (ULIRGs), reaching IR luminosities ($L_{\rm IR}$) of $L_{\rm IR} > 10^{12}\,{\rm L}_{\odot}$ (Kovács et al. 2006; Coppin et al. 2008; Hayward et al. 2011). Spectroscopic surveys targeting the redshift distributions of SMGs indicate that the bulk of the DSFGs population peaks at $z \sim 2$–4 (e.g. Chapman et al. 2005; Strandet et al. 2016), encompassing the peaks of supermassive black hole (SMBH) accretion (Cattaneo & Bernardi 2003; Hopkins, Richards & Hernquist 2007) and cosmic star formation activity (Madau & Dickinson 2014). However, a significant tail of higher redshift DSFGs appears to be already in place at $z > 5$ (e.g. Walter et al. 2012; Riechers et al. 2013, 2017; Weiß et al. 2013; Strandet et al. 2017). The latter are often found to be extreme hyperluminous IR galaxies (HyLIRGs), reaching infrared luminosities of $L_{\rm IR} > 10^{13}\,{\rm L}_{\odot}$ and star formation rates (SFRs) exceeding $1000\,{\rm M}_{\odot}\,{\rm yr}^{-1}$, likely tracing the result of strong dynamical interactions (i.e. major mergers) and intense gas accretion events occurring in the densest regions of the early Universe (e.g. Capak et al. 2011; Ivison et al. 2011; Riechers et al. 2011, 2017; Oteo et al. 2016; Pavesi et al. 2018). Recently, Marrone et al. (2018) reported high-resolution Atacama Large Millimeter/submillimeter Array (ALMA) observations of SPT0311-58, a IR-luminous system at $z = 6.9$, originally identified in the $2500\,{\rm deg}^2$ South Pole Telescope (SPT) survey (Carlstrom et al. 2011). ALMA reveals this source to be a pair of interacting extremely massive and IR-luminous star-bursting galaxies: SPT0311-58W, an HyLIRG with $L_{\rm IR} = 3.3 \pm 0.7 \times 10^{13}\,{\rm L}_{\odot}$ and an SFR $\sim 2900\,{\rm M}_{\odot}\,{\rm yr}^{-1}$, and SPT0311-58E, a ULIRG with $L_{\rm IR} = 4.6 \pm 1.2 \times 10^{12}\,{\rm L}_{\odot}$ and SFR $\sim 540\,{\rm M}_{\odot}\,{\rm yr}^{-1}$. Using

★ E-mail: michele.ginolfi@oa-roma.inaf.it, michele.ginolfi@inaf.it

different proxies, Marrone et al. (2018) estimated the DM halo mass hosting this system to be $M_{\rm DM} = (1.4–7) \times 10^{12}$ M$_\odot$, showing that SPT0311-58 marks a rare peak in the cosmic density field at this early cosmic time and it lies close to the exclusion curve predicted by the current structure formation paradigm.

Many models of SMBH galaxy co-evolution suggest an evolutionary link between ULIRGs and quasars (quasars; Sanders et al. 1988a,b; Silk & Rees 1998; Di Matteo, Springel & Hernquist 2005; Springel et al. 2005; Hopkins et al. 2006, 2008, and Alexander & Hickox 2012 for a review). ULIRGs may represent the initial, heavily obscured, stages of quasars, which, after shedding the surrounding dust through energetic galaxy-scale outflows (e.g. Harrison et al. 2012; Maiolino et al. 2012; Fan et al. 2018), evolve into a ultraviolet (UV)/optical bright unobscured phase. In this work, we explore the hierarchical merger histories of $z \sim 6$ quasars to investigate their connection with ULIRGs and HyLIRGs. To this aim, we use GAMETE/QSOdust (hereafter GQd, Valiante et al. 2014, 2016), a semi-analytic model tested to reproduce the observed properties of a sample of high-z quasars (Valiante et al. 2014). GQd consistently follows the formation and evolution of nuclear black holes (BHs) and their host galaxies, accounting for star formation, interstellar medium (ISM) chemical evolution (metals and dust) and mechanical feedback, along different merger histories of the parent DM halo. Therefore, GQd is a suitable tool to (i) investigate the physical properties of the ancestors at $z \sim 7–9$ of luminous quasars at $z \sim 6$; (ii) statistically quantify the number density of expected ULIRG and HyLIRG progenitors, and (iii) probe whether $z \sim 6$ luminous quasars can be the signposts of the rare peaks in the cosmic density field observed at $z \sim 7$ (i.e. Marrone et al. 2018). The paper is organized as follows. In Section 2, we briefly describe the GQd model. Sections 3 and 4 show the results of this work and a discussion of their implications. Throughout the paper, we assume a ΛCDM cosmology with $\Omega_{\rm m} = 0.24$, $\Omega_\Lambda = 0.76$, $\Omega_{\rm b} = 0.04$, and $H_0 = 73\,{\rm km\,s^{-1}\,Mpc^{-1}}$.

2 MODEL DESCRIPTION

GQd [1] is a semi-analytic, data-constrained model aimed at studying the formation and evolution of high-redshift quasars and their host galaxies in a cosmological framework. In this section we summarize the main features of GAMETE/QSOdust, referring the reader to Valiante et al. (2011, 2014, 2016) for a thorough description of the model. GQd has been tested to reproduce the observed properties of quasars at $z > 5$, such as the BH mass, the molecular gas, and dust masses in the ISM (Valiante et al. 2014). Following Valiante et al. (2016), in this work we focus on the evolution of an SDSS J1148 + 5251 (hereafter J1148)-like quasar at $z = 6.4$, one of the best-studied high-z luminous quasars[2] (e.g. Willott, McLure & Jarvis 2003; Walter et al. 2004; Maiolino et al. 2005; Cicone et al. 2015; see Table 1.), and we use it as a prototype for the general class of luminous $z \sim 6$ quasars.

The hierarchical merger history

We first reconstruct different hierarchical merger histories (merger trees) of an $M_{\rm DM} = 10^{13}$ M$_\odot$ DM halo hosting a J1148-like quasar at $z = 6.4$, using a binary Monte Carlo algorithm accounting for mass infall (e.g. Volonteri, Haardt & Madau 2003), based on the Extended Press-Schechter theory (e.g. Lacey & Cole 1993). This approach enables us to produce a large (statistically meaningful) number of random, semi-analytical merger trees of the same DM halo, simultaneously resolving the first collapsed objects. The DM resolution mass, $M_{\rm res}$, is chosen to resolve the first collapsed objects where the gas is able to cool and form stars, i.e. the so-called *mini-haloes*, with masses of $M_{\rm h} \sim 10^6$ M$_\odot$ and virial temperatures of $T_{\rm vir} < 10^4$ K (see Bromm 2013 for a review). Given this requirement, we simulate the merger trees adopting an $M_{\rm res}$ of

$$M_{\rm res}(z_i) = 10^{-3}\, M_h(z_0) \left(\frac{1+z_i}{1+z_0}\right)^{-7.5}, \quad (1)$$

where $M_h(z_0)$ is the host DM halo at redshift $z_0 = 6.4$. Mini-haloes dominate the halo mass spectrum at very high-z; at $z \lesssim 14$ the merger tree halo population is dominated instead by Lyα-cooling haloes, namely DM haloes with $T_{\rm vir} \geq 10^4$ K (see Valiante et al. 2016 for details). By construction, the entire population of haloes along the merger trees, that we call *progenitors*, contribute to assembling the simulated quasar host galaxies. However, when specified within the text, we will restrict the analysis to massive progenitors, hosted by DM haloes with $M_{\rm DM} > 10^{11}$M$_\odot$. This mass selection, as discussed in Section 3, reflects our interest of studying the most IR-luminous galaxies in the simulation.

Table 1. Observed and inferred properties of the quasar SDSS J1148 + 5251 at $z = 6.42$.

$L_{\rm FIR}$[a] (10^{13} L$_\odot$)	$L_{\rm bol}$[b] (10^{14} L$_\odot$)	SFR[a] (10^3M$_\odot$yr^{-1})	$M_{\rm dust}$[a] (10^8 M$_\odot$)	$M_{\rm BH}$[c] (10^9 M$_\odot$)
2.2 ± 0.33	1.36 ± 0.74	2.0 ± 0.5	$3.4^{+1.38}_{-1.54}$	4.9 ± 2.5

[a]The values of $L_{\rm FIR}$, SFR, and $M_{\rm dust}$ have been computed by Valiante et al. (2011, 2014).
[b]The bolometric luminosity, $L_{\rm bol}$, is estimated from the observed flux at 1450 Å (Fan et al. 2003) using the bolometric correction by Richards et al. (2006).
[c]The black hole mass, $M_{\rm BH}$, is estimated from the Mg$_{\rm II}$ doublet and the $\lambda = \sim$3000 Å continuum (De Rosa et al. 2011).

BH growth and baryonic evolution

Merger trees are used as an input to reconstruct the formation and evolution of the J1148-like quasar and its host galaxy through cosmic time. The baryonic evolution inside each progenitor galaxy is regulated by processes of star formation, BH growth and feedback, and followed consistently through the cosmic mass assembly. BHs growth is driven by (i) *mergers:* we assume that in major mergers[3] the BHs present in the nuclei of the two interacting galaxies coalesce, forming a new more massive BH. In minor mergers, the merger time-scale of the two BHs is of the order of the Hubble time or longer (see e.g. Tanaka & Haiman 2009). The less massive BH of the merging pair is assumed to remain as a satellite and we do not follow its evolution. (ii) *gas accretion:* the accretion rate is described by a modified[4] Bondi–Hoyle–Lyttleton formula, capped at the Eddington rate (see Valiante et al. 2014 for details). We find that, while BH growth is mostly driven by mergers at very high-z (i.e.

[1]The model GAMETE (GAlaxy MErger Tree and Evolution) was originally developed to study the formation and cosmological evolution of local, Milky Way like galaxies (Salvadori, Schneider & Ferrara 2007; Salvadori, Ferrara & Schneider 2008).
[2]Absolute AB magnitude of the continuum in the rest-frame at 1450 Å of $M_{1450} = -27.82$ (Fan et al. 2003).
[3]A major merger occurs when two DM haloes with mass ratio (less massive over the most massive) $\mu > 1/4$ coalesce.
[4]We re-scaled by a factor $\alpha_{\rm BH} = 50$, to account for the higher central densities around accreting BHs (e.g. Di Matteo et al. 2005).

$z \gtrsim 11$), gas accretion is the dominant growth mode at lower redshifts (Valiante et al. 2016). At each snapshot of the merger tree, stars in the progenitor galaxies form according to an SFR proportional to the available gas mass, with an efficiency that is enhanced during major mergers (see Valiante et al. 2014). Following star formation, supernovae (SNe) and asymptotic giant branch stars (AGB) progressively enrich the ISM of each galaxy with metals and dust according to their specific mass and metallicity-dependent yields and to their evolutionary time-scales. We follow the life-cycle of metals and dust including physical prescriptions for dust processing in a two-phase ISM: SN shocks can destroy dust grains in the hot, diffuse medium while dust grains can grow in mass by accreting gas-phase heavy elements in the cold medium (see Valiante et al. 2014 and de Bennassuti et al. 2014, for details). A fraction of the energy released by SN explosions (0.2 per cent) and BH accretion (0.25 per cent) is converted into kinetic energy of the gas in the host galaxy, driving gas outflows in the form of winds. While these efficiencies are lower than what is generally adopted in hydrodynamical simulations[5] the predicted strength of mechanical feedback is in good agreement with observations of the outflowing gas in J1148 (Maiolino et al. 2005, 2012; Valiante et al. 2012; Cicone et al. 2015; see also Bischetti et al. 2018, who carry out a stacking analysis of a sample of 48 quasars at $4.5 < z < 7.1$ detected by ALMA in the [C II] 158 μm line, and find an outflow kinetic power that is ∼0.1 per cent of the AGN luminosity).

3 THE IR PROPERTIES OF MASSIVE PROGENITORS OF HIGH-Z QUASAR HOST GALAXIES

We calculate the IR luminosity of each galaxy by assuming that in the Rayleigh–Jeans part of the spectrum (in the limit of small frequencies, that is $h\nu \ll k_B T$), dust radiates as a 'grey-body' with an opacity coefficient per unit dust mass, $k_d(\nu) = k_0 \sim (\nu/\nu_0)^\beta$, where ν_0, k_0, β depend on the adopted model of dust. Integrating over the IR wavelength range 8–1000 μm (300−38 000 GHz), we compute the corresponding L_{IR} as,

$$L_{IR} = 4\pi M_{dust} \int k_d(\nu)\, B(\nu, T_{dust})\, d\nu, \quad (2)$$

where $B(\nu, T_{dust})$ is the Planck function for a dust temperature T_{dust}. We estimate L_{IR}, averaging over seven different models of dust composition[6] (each of them providing a unique combination of the parameters k_0, ν_0, β; see Table 2) and we vary the dust temperature[7] in the range $T_{dust} = [35 - 55]$ K.

[5]In one of the most popular descriptions of AGN-driven winds in hydrodynamical simulations, 5 per cent of the radiation energy is thermally coupled to the surrounding gas (Di Matteo et al. 2005). This difference may be due to the complex interaction of the outflow with the inhomogeneous ISM and the effects of radiative losses that cannot be captured by our simple semi-analytical model.

[6]Following Valiante et al. (2011) we use models of dust composition from Bertoldi et al. (2003), Robson et al. (2004), Beelen et al. (2006), Weingartner & Draine (2001), Bianchi & Schneider (2007). In addition, we also consider the more recent 'AC' model by Galliano et al. (2011) and 'THEMIS' by Jones et al. (2017) (see the review by Galliano, Galametz & Jones 2018 for a discussion).

[7]Warm interstellar dust, associated to starburst regions, dominates the emission in the rest-frame far-IR (Dunne et al. 2000; Wang et al. 2008; Valiante et al. 2016).

Table 2. Compilation of the k_0, λ_0, and β parameters, defining the opacity coefficient per unit dust mass in the different models of dust composition used in this work.

Model (reference)	k_0 (cm^2 gr^{-1})	λ_0 (μm)	β (β)
Bertoldi et al. (2003)	7.5	230	1.5
Robson et al. (2004)	30	125	2.0
Beelen et al. (2006)	0.4	1200	1.6
Weingartner & Draine (2001)[a]	34.7	100	2.2
Bianchi & Schneider (2007)	40	100	1.4
THEMIS - Jones et al. (2017)	6.4	250	1.79
AC - Galliano et al. (2011)	16	160	1.7

[a]Fit to the model for the Small Magellanic Cloud in the spectral range (40–200) μm.

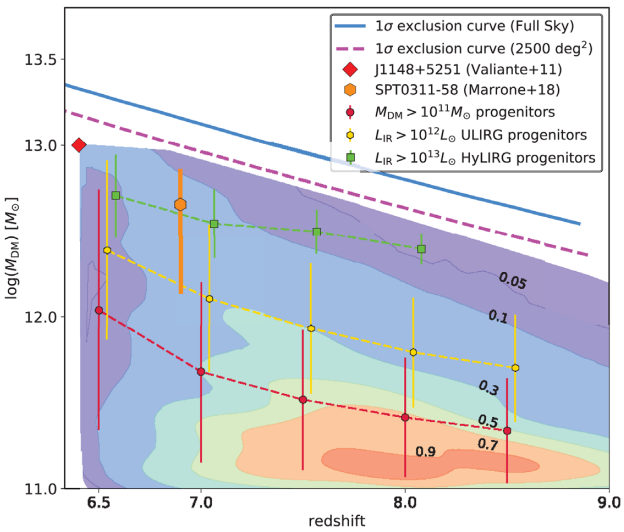

Figure 1. Density plot showing the M_{DM} distribution of DM haloes hosting massive progenitor galaxies ($M_{DM} > 10^{11}$ M$_\odot$) of a J1148-like quasar host galaxy (the red point), in the redshift interval $6.4 < z < 9$. The density distribution is based on the total statistics of 10 different merger trees (see Section 2); the percentile levels are marked by the filled colour contours and labelled in the figure. The red dashed line and points represent the redshift evolution of the averaged M_{DM} of all massive progenitors ($M_{DM} > 10^{11}$ M$_\odot$). The gold and green lines and points represent the redshift evolution of the average M_{DM} of haloes hosting massive progenitors with $L_{IR} > 10^{12}$ L$_\odot$ (ULIRGs) and $L_{IR} > 10^{13}$ L$_\odot$ (HyLIRGs), respectively. Error bars are indicative of the 1σ standard deviation calculated in equispaced redshift bins (the slight offset of the bins position for red, gold, and green points has been introduced to avoid overlapping and help visualization). The orange point represents the DM halo mass hosting the HyLIRG system SPT0311-58, at $z = 6.9$ (Marrone et al. 2018). The blue solid and magenta dashed lines represent the 1σ exclusion curves, i.e. the most massive haloes that are expected to be observable within the whole sky and a 2500 deg^2 area (the size of the SPT survey in which SPT0311-58 was identified), respectively, as a function of redshift (Harrison & Hotchkiss 2013; Marrone et al. 2018).

Figs 1 and 2 show, respectively, (i) the redshift distribution of simulated DM halo masses and (ii) the IR luminosities of massive progenitors ($M_{DM} > 10^{11}$M$_\odot$) of J1148-like quasar host galaxies at $z \sim 6.4$, in all the simulated merger trees. Fig. 1 shows that, although the bulk of the mass distribution of massive progenitors is concentrated in the mass range $11 < \log(M_{DM}/M_\odot) < 12$ (especially at $z \sim 8$; see percentile levels in the density plot), IR-luminous galaxies with $L_{IR} > 10^{12}$ L$_\odot$ occupy DM haloes with $M_{DM} > 10^{12}$ M$_\odot$, at

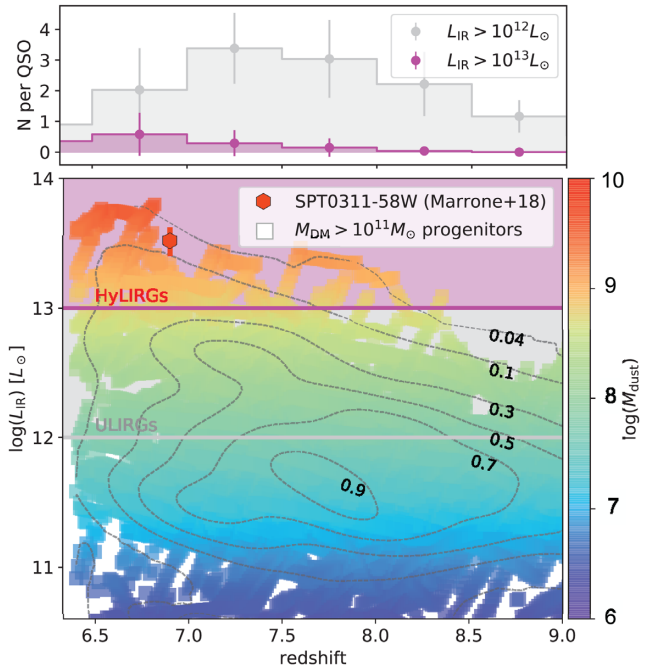

Figure 2. *Bottom panel:* redshift distribution of the L_{IR} in massive progenitors ($M_{DM} > 10^{11}$ M$_\odot$) of a J1148-like quasar host galaxy, in the redshift interval $6.4 < z < 9$, using the total statistics of 10 independent merger trees. The distribution is colour-coded depending on the galaxy ISM dust mass. The black dashed lines represent the density contours with the corresponding percentiles labelled in the figure. The grey (magenta) filled regions define the L_{IR} range of ULIRGs (HyLIRGs). The red point represents the L_{IR} of SPT0311-58W, the most massive galaxy in the interacting system SPT0311-58 (Marrone et al. 2018). *Top panel:* average number of ULIRGs (the grey points) and HyLIRGs (the magenta points) at $6.4 < z < 9$, expected for each luminous quasar at $z \sim 6$. Error-bars are indicative of the $\sim 1\sigma$ standard deviation calculated over 10 different merger trees.

least in the redshift interval $6.4 < z < 7.5$. In particular, we find that galaxies with HyLIRGs-like luminosity ($L_{IR} > 10^{13}$ L$_\odot$, consistent with the IR luminosity measured in SPT0311-58W; Marrone et al. 2018) reside in the most massive haloes, with masses of about $M_{DM} \sim 10^{12.5} - 10^{13}$ M$_\odot$, consistent with the dynamical mass inferred for the interacting system SPT0311-58 (see the orange hexagon in Fig. 1). These findings indicate that exceptionally massive DM haloes hosting HyLIRGs, as the $\sim 10^{12.6}$ M$_\odot$ halo hosting SPT0311-58 at $z \sim 7$, can be found within the family tree of UV/optical bright quasars at $z \sim 6$. In the next paragraphs, we explore the expected physical properties of the IR-luminous progenitors of high-z luminous quasar host galaxies, as well as their frequency (i.e. the expected number per quasar) and their observability in the mm and X-ray bands.

3.1 How many IR-luminous progenitor galaxies do we expect for each $z \sim 6$ luminous quasar?

In the top panel of Fig. 2 we show the predicted number of IR-luminous progenitor galaxies in the redshift interval $6.4 < z < 9$ expected for each luminous J1148-like quasar at $z \sim 6.4$. Each high-z luminous quasar has, on average, about 2.8 ULIRG progenitors with $L_{IR} > 10^{12}$ L$_\odot$, and about 0.4 HyLIRG progenitors with $L_{IR} > 10^{13}$ L$_\odot$, between $z \sim 6 - 8$. Recently, Jiang et al. (2016) using a complete sample of 52 quasars at $z > 5.7$ selected from the Sloan Digital Sky Survey (SDSS), spanning a wide luminosity range of $-29.0 \leq M_{1450} \leq -24.5$, found that the number density of bright quasars with $M_{1450} < -26.7$ at $z \sim 6$ is (0.4 ± 0.1) Gpc^{-3}.[8] Combining this information with our estimate of the number of expected IR-luminous progenitor galaxies per quasar, we predict the spatial number density of HyLIRG (ULIRG) progenitors to be about 0.16 ± 0.08 (1.2 ± 0.6) Gpc^{-3} in the redshift range $z \sim 6$–8. Since these values refer to the population of ULIRGs/HyLIRGs found within the merger trees of UV/optical bright quasars at $z \sim 6$, they provide lower limits on the effective number density of the overall population of IR-luminous galaxies at $z > 6$. Potential deviations might be also driven by the effect of the duty cycle on the number counting of high-z quasars, resulting in a systematic underestimation of their number densities in large single-epoch imaging surveys (see e.g. Romano-Diaz et al. 2011). An alternative way to estimate the number density of the overall population of IR-luminous galaxies at $z > 6$ comes from our finding that, at $6.5 < z < 8$, the most massive DM haloes ($M_{DM} > 10^{12.5}$ M$_\odot$) in the merger trees of simulated quasars are most likely to host HyLIRGs (see Fig. 1). Assuming that this finding can be extended to all DM haloes in the same mass regime (i.e. also haloes that are not expected to evolve in a quasar at $z \sim 6$), then the number density of the HyLIRGs population should be consistent with the number density of DM haloes with $M_{DM} > 10^{12.5}$ M$_\odot$ predicted by the ΛCDM cosmology[9] at $6.5 < z < 8$, i.e. about 2 Gpc^{-3}.

Fig. 2 also shows that HyLIRGs are characterized by dust masses $\gtrsim 10^{8.7}$ M$_\odot$ already at $z \sim 8$–8.5, while ULIRGs have dust masses in the range $10^{7.5} < M_{dust}/M_\odot < 10^9$. Despite their large stellar masses, $\gtrsim$70 per cent of the dust mass has formed in the ISM of these galaxies through processes involving some form of grain growth[10] (see Valiante et al. 2011, where the maximum dust masses obtained from stellar sources, e.g. SNe and AGB stars, is calculated as a function of M_{star}, under the conservative assumption that dust grains are not destroyed by interstellar shocks).

3.2 The physical properties of high-z HyLIRGs

In Fig. 3 we show the redshift, stellar mass (M_{star}), gas mass (M_{gas}), SFR, dust mass (M_{dust}), metallicity (Z), and BH mass (M_{BH}) distributions of HyLIRG progenitors (magenta histograms) of high-z quasars. We find that HyLIRG progenitors are generally highly massive (i.e. $M_{star} \sim 10^{11}$–10^{12} M$_\odot$; Fig. 3b), gas rich (i.e. $M_{gas} \sim 10^{10.5}$–$10^{11.5}$ M$_\odot$; Fig. 3c) systems. They experience strong starbursts, with SFRs $\sim 10^2$–10^4 M$_\odot$ yr^{-1} (see Fig. 3d), enabling them to reach supersolar metallicities (see Fig. 3e), and large dust masses (i.e. $M_{dust} \sim 10^9$ M$_\odot$; Fig. 3f) already at $z \sim 6.5$–7.5. The same properties are also shown for galaxies experiencing mergers with HyLIRG companions along the merger trees (the light green histograms). Those galaxies are found to have different properties than HyLIRGs (note the different x-axis range between magenta and green histograms in Fig. 3). In particular, we find that the bulk of the population of interacting companions is generally less massive (the M_{star} distribution peaks at $M_{star} \sim 10^9$ M$_\odot$), less star-forming

[8]This value is consistent with the estimates provided by previous works, e.g. Fan et al. (2004) and Willott et al. (2010).
[9]The ΛCDM-predicted number density of DM haloes was obtained using HMF*calc*, publicly available at http://hmf.icrar.org/ (see Murray, Power & Robotham 2013).
[10]We note that the efficiency and even the physical nature of grain growth is still an active subject of study (e.g. Zhukovska et al. 2016; Ceccarelli et al. 2018; Ginolfi et al. 2018).

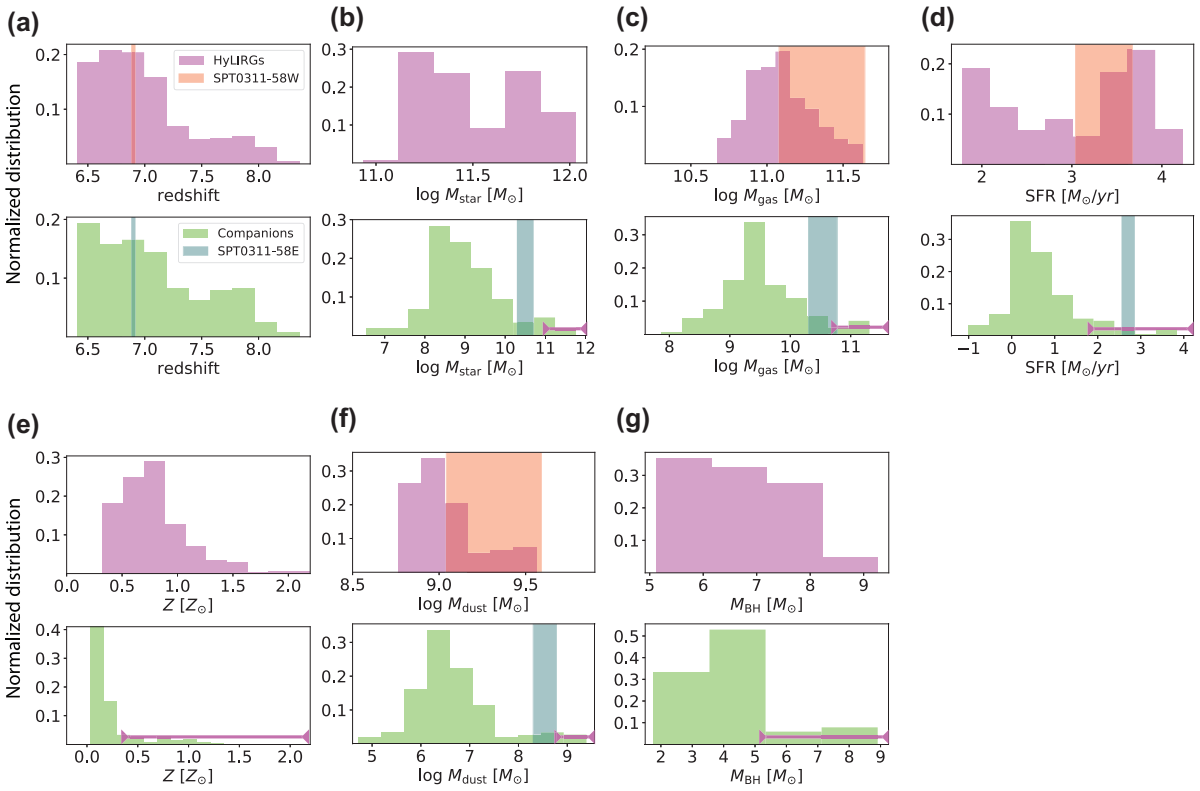

Figure 3. The magenta histograms show the distributions of physical properties (M_{star}, M_{gas}, SFR, Z, M_{dust}, M_{BH}) and redshift of HyLIRGs progenitors of $z \sim 6$ quasars (namely the galaxies included in the magenta-filled region of Fig. 2). The light green histograms show the same distributions for systems experiencing mergers with HyLIRGs progenitors. The overlaid magenta lines indicate the range of values of HyLIRGs properties, revealing clear differences between HyLIRGs and their interacting companions. The overlaid red and dark green solid areas indicate the observed values of the two galaxies composing the interacting system observed by Marrone et al. (2018), i.e. SPT0311-58W and SPT0311-58E, respectively. The width of the area is representative of the uncertainty on the measurements.

(the SFR distribution peaks at SFR $\sim 5\ M_\odot\ yr^{-1}$) and less chemically evolved (i.e. subsolar metallicities and $M_{dust} \sim 10^{6.5}\,M_\odot$). However, we find that the tails of the distributions of interacting companions extend towards the HyLIRG regime, as shown by the intersections between the light green histograms and the magenta lines in Fig. 3. The existence of this channel of interaction is crucial from the point of view of evolutionary models of SMBH–galaxy co-evolution: in fact, gas-rich major mergers are thought to be an efficient mechanism to deliver cold gas at the centre of the resulting halo and therefore fuel the growth of the SMBH and trigger AGN activity (Di Matteo et al. 2005; Hopkins et al. 2008; Pezzulli, Valiante & Schneider 2016).

3.3 The observability of high-z HyLIRGs with ALMA

By assuming an optically thin, $\tau_d(\lambda) < <1$, rest-frame far-IR emission, the intrinsic flux observed in a given band F_ν can be estimated as,

$$F_\nu = \frac{M_{dust}\, k_d(\nu)\, B(\nu, T_{dust})\,(1+z)}{d_L^2(z)}, \tag{3}$$

where $d_L^2(z)$ is the luminosity distance of a source at given redshift. However, it is well known that at high redshift the cosmic microwave background (CMB) is hotter and brighter. Its temperature, $T_{CMB}(z) = T_{CMB}^{z=0}\,(1+z)$, at $z > 5$ approaches the temperature of the cold dust, decreasing the contrast of the intrinsic rest-frame IR emission against the CMB. To account for this effect, we adopted the results by da Cunha et al. (2013), who provided general correction factors to estimate what fraction of the dust emission can be detected against the CMB as a function of frequency, redshift, and temperature,

$$\frac{F_\nu^{\text{against CMB}}}{F_\nu^{\text{intrinsic}}} = 1 - \frac{B(\nu, T_{CMB}(z))}{B(\nu, T_{dust}(z))}. \tag{4}$$

It follows from equation (4) that the flux–CMB contrast increases at higher T_{dust} (see also the discussion in da Cunha et al. 2013). This is the case for our simulated HyLIRGs, where the interstellar dust in the warm phases of the ISM is heated by the vigorous starburst activity, reaching the high-temperature values adopted in this paper ($T_{dust} \gtrsim 40$ K, see also Dunne et al. 2000; Wang et al. 2008; Valiante et al. 2016). Indeed we find that a large fraction, namely 70–80 per cent, of the intrinsic rest-frame IR emission can be detected against the CMB. Fig. 4 shows the distribution (both averaged values and dispersions) of the rest-frame IR fluxes (*CMB-corrected*) for HyLIRG progenitors at $6.4 < z < 9$. Fluxes are calculated in the ALMA Bands [8, 7, 6, 4, 3], respectively, centred at observed-frame wavelengths [0.7, 0.95, 1.25, 2, 3] mm, and range from a minimum value of 0.2 mJy at 3 mm (Band 3), to a maximum value of 50 mJy at 0.7 mm (Band 8). We calculated the *on-source* integration times[11] needed to detect the estimated continuum fluxes

[11] The *on-source* integration times were obtained using the ALMA Cycle 6 sensitivity calculator.

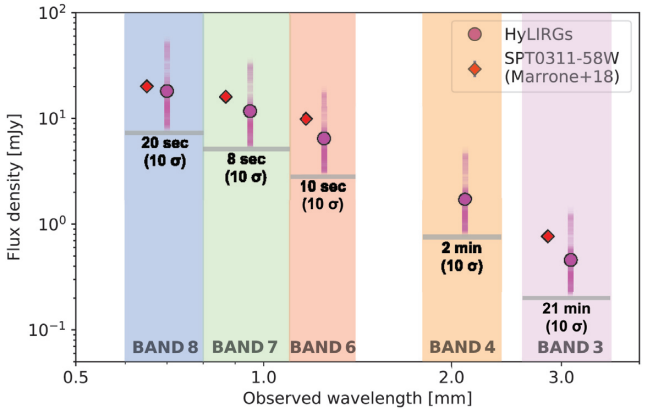

Figure 4. Rest-frame far-IR fluxes of HyLIRG progenitors of a J1140-like quasar host galaxy. Fluxes are calculated in the ALMA Bands [8, 7, 6, 4, 3] (the coloured filled regions), respectively, centred at observed-frame [0.7, 0.95, 1.25, 2, 3] mm. The magenta points represent the averaged values of the HyLIRGs population, and bars represent their dispersions (the colour intensity traces the flux distribution at any given wavelength bin). The red points represent the fluxes of SPT0311-58W (Marrone et al. 2018) in the ALMA Bands [8, 7, 6, 4, 3]. For fluxes corresponding to the grey bars, located at the low-end of the HyLIRG flux distributions at any wavelength bin, we report the on-source observing time needed by ALMA to reach an S/N $= 10\sigma$.

with a signal-to-noise ratio of S/N = 10. We find that HyLIRGs progenitors of high-z quasar host galaxies can be easily detected with ALMA with a modest amount of observing time, ranging from few second in Bands 6-7-8, to ∼20 min in Band 3 (see Fig. 4). We note that, although for such short integrations most of the time is dedicated to the instrumental setup and calibrations, the total integration time (including overheads) needed to reach the required sensitivity is less than 30 min in all the Bands.

3.4 The X-ray observability of BH activity in high-z HyLIRGs

As shown in Fig. 3(g), we find that the HyLIRG progenitors of luminous high-z quasars, host nuclear BHs with an almost uniform distribution of masses in the range $10^5\,M_\odot < M_{\rm BH} < 10^8\,M_\odot$, and a high-mass tail at $M_{\rm BH} \lesssim 10^9\,M_\odot$ (populated by systems in the last steps of the merger trees). Such a broad range of nuclear BH masses results from the diversity of merging and accretion histories predicted by the model. To assess the possibility of detecting BH activity in the nuclei of high-z HyLIRGs, we compared the predicted X-ray luminosity in the (observed-frame) soft ([0.5–2] keV) and hard ([2–10] keV) X-ray bands with the flux limits of recent surveys. Following Pezzulli et al. (2017), we modelled the X-ray luminosity of accreting BHs considering the primary emission from the hot corona and the reflection component due to the surrounding neutral medium. The first one is parametrized as a power law, $L_\nu \propto \nu^{-\Gamma+1} e^{h\nu/Ec}$, with an exponential cut-off energy of $E_c = 300$ keV (Sazonov, Ostriker & Sunyaev 2004; Yue et al. 2013) and photon spectral index $\Gamma = 0.32 \log \lambda_{\rm Edd} + 2.27$, that we assume to depend on the Eddington ratio $\lambda_{\rm Edd} = L_{\rm bol}/L_{\rm Edd}$ (Brightman et al. 2013). The metallicity-dependent reflection component is computed using the PEXRAV model (Magdziarz & Zdziarski 1995) in the XSPEC code.[12] The metallicity and Eddington ratio

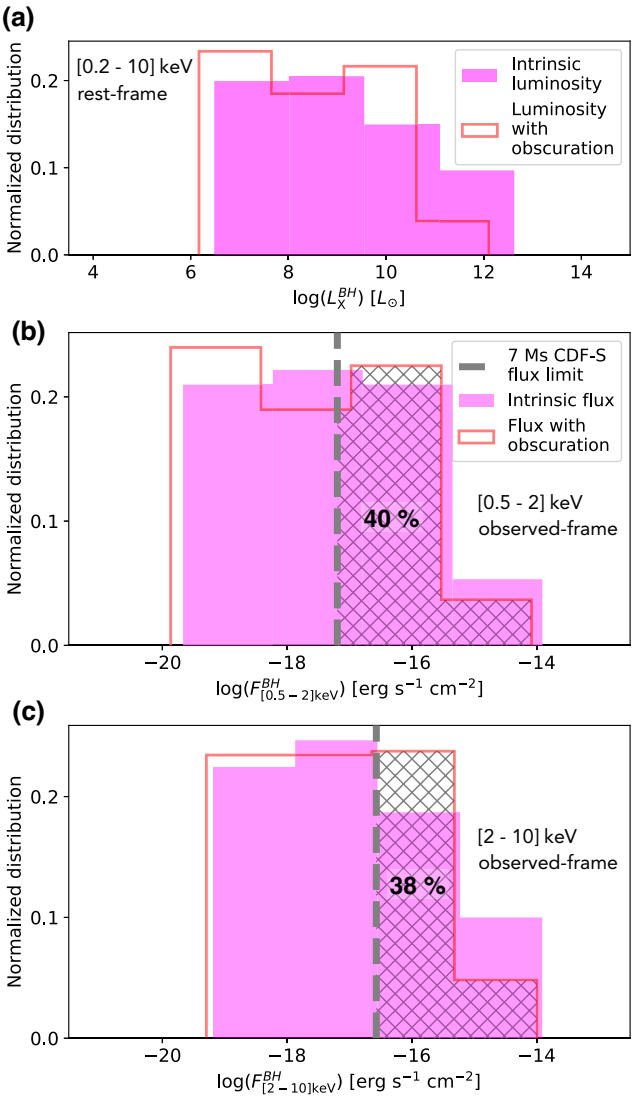

Figure 5. (a) Distribution of the intrinsic (the magenta histogram) and obscured (the red histogram) X-ray luminosities (integrated over the rest-frame soft + hard band, [0.2–10] keV) produced by the accreting BHs in the HyLIRG progenitors of high-z quasars. (b) and (c) Distributions of the intrinsic and obscured X-ray fluxes produced by the accreting BHs, in the observed-frame soft (panel b) and hard (panel c) X-ray bands. The grey dashed lines represent the flux limits of the 7 Ms CDF-S survey, i.e. $F_{\rm CDF-S} = 6.4 \times 10^{-18}$ erg s^{-1} cm^{-2} in the soft band, and $F_{\rm CDF-S} = 2.7 \times 10^{-17}$ erg s^{-1} cm^{-2} in the hard band. About 40 per cent (38 per cent) of the HyLIRGs population shows a detectable $F_{\rm X}^{\rm BH}$ in the observed-frame soft (hard) band (hatched regions).

$\lambda_{\rm Edd} = L_{\rm bol}/L_{\rm Edd}$ are computed using the values predicted by GQd for each accreting BH. We find that the BH activity in HyLIRGs generates an intrinsic emission corresponding to X-ray luminosities (integrated over the rest-frame [0.5–10] keV band) of $L_{\rm X}^{\rm BH} = [10^{6.5}-10^{12.5}]$ L$_\odot$ (see Fig. 5a), and to intrinsic fluxes $F_{\rm X}^{\rm BH} = [10^{-20}-10^{-14}]$ erg s^{-1} cm^{-2} in the observed-frame soft/hard bands (see flux distributions in Figs 5b and c). The intrinsic X-rays flux is attenuated by the interaction of the radiation produced during the

[12]The reflection component is computed assuming an isotropic source located above the disc, fixing the reflection solid angle to 2π, the inclination angle to 60°, and the reflection strength parameter to $R = 1$, consistent with typical values of local AGNs (Zappacosta et al. 2018).

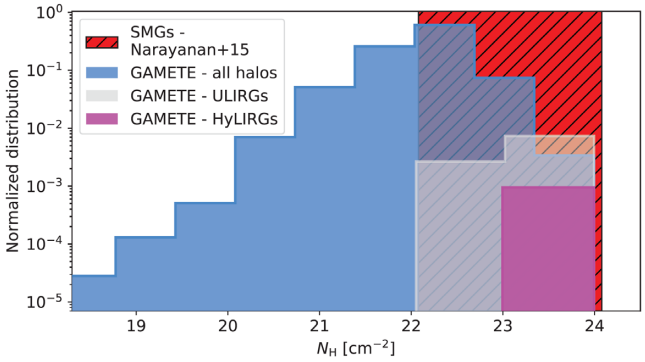

Figure 6. The blue histogram shows the distribution of N_H predicted for the overall population of galaxies in our model, while the grey and magenta histograms show the distribution of N_H predicted for the ULIRG and HyLIRG progenitors of the $z \sim 6$ quasar host galaxies, respectively. The N_H distribution for ULIRGs is consistent with the distribution of N_H predicted for SMGs by the cosmological hydrodynamical simulation by Narayanan et al. (2015) (the red hatched region).

BH accretion with the gas and dust in the immediate surroundings of the BH (mainly photoelectric absorption and Compton scattering of photons against free electrons). For this reason the effect of obscuration has to be taken into account, and the obscured emerging flux can be written as $F_\nu^{abs} = F_\nu^{unabs}\, e^{-\tau_\nu}$; at energies $E \gtrsim 0.1$ keV, assuming a fully ionized H–He mixture, the optical depth τ_ν is (Yaqoob 1997)

$$\tau_\nu = (1.2\,\sigma_T + \sigma_{ph})\, N_H, \quad (5)$$

where N_H is the hydrogen column density, while σ_T and σ_{ph} are the Thomson and photoelectric cross-section, respectively (see Pezzulli et al. 2017 for a description of σ_{ph} and its dependence on energy and metallicity). We computed N_H assuming the gas to be distributed following a singular isothermal sphere profile (see Valiante et al. 2016),

$$\rho(r) = \frac{\rho_0}{1 + (\frac{r}{r_{core}})^2}, \quad (6)$$

where the normalization factor ρ_0 is a function of M_{gas}, the virial radius (R_{vir}), and the core radius (r_{core}). By assuming $r_{core} = 50$ pc, we find that our simulated ULIRGs have $N_H = \sim[10^{22}-10^{24}]$ cm^{-2}, in the same range predicted by cosmological hydrodynamical simulations for high-z SMGs (e.g. Narayanan et al. 2015; see Fig. 6). Adopting the same r_{core}, we find that HyLIRG progenitors have $N_H \sim [10^{23} - 10^{24}]$ cm^{-2}. As shown in Figs 5(b) and (c), the resulting net attenuation of fluxes by obscuration in the observed-frame soft X-ray band is about a factor of 2, while fluxes in the observed-frame hard X-ray band are almost unaffected by attenuation. This can be explained in terms of the photoelectric cross-section decreasing for increasing energy (see a thorough discussion in Pezzulli et al. 2017). Finally, we compared the predicted, obscuration-attenuated F_X^{BH} with the flux limits obtained by *Chandra* observations of the recent 7 Ms *Chandra* Deep Field South Survey (7 Ms CDF-S; Luo et al. 2017), i.e. $F_{CDF-S} = 6.4 \times 10^{-18}$ erg s^{-1} cm^{-2} in the soft band and $F_{CDF-S} = 2.7 \times 10^{-17}$ erg s^{-1} cm^{-2} in the hard band. We find that in both bands, a significant fraction of our simulated HyLIRGs population has a potentially detectable F_X^{BH} (40 per cent and 38 per cent, respectively; see hatched regions of the red histograms in Figs 5(b) and (c). To test if F_X can be considered as a tracer of nuclear activity in high-z HyLIRGs, we estimated the contribution of SFR-related (e.g. X-ray binary populations; XRBs) processes to the X-ray luminosity, L_X^{SFR}, by using the redshift-dependent scaling relation between the rest-frame hard L_X and SFR, found by Lehmer et al. (2016):

$$\log(L_X^{SFR})_{[2-10]\,keV} = 39.82 + 0.63\log(SFR) + 1.31\log(1+z).$$

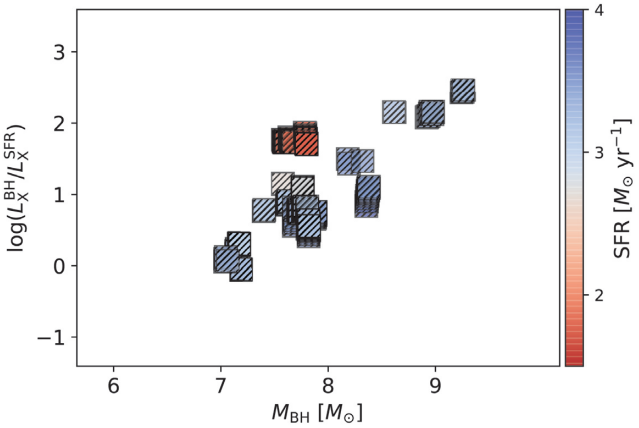

Figure 7. The relative contribution of rest-frame hard X-ray emission produced by nuclear activity and stars is shown as a function of M_{BH} and colour coded depending on the SFR, for galaxies with a detectable observed-frame soft X-ray flux (namely the objects in the red hatched region of Fig. 5b). At $M_{BH} \gtrsim 10^7$ M$_\odot$, the X-ray emission produced by accreting SMBHs dominates over the X-ray emission produced by stars. For about 40 per cent of the population, $\log(L_X^{BH}/L_X^{SFR}) > 1$.

In Fig. 7, we show the relative contribution between the X-ray luminosity produced by the accreting SMBHs (once the attenuation by obscuration has been considered) and by XRBs, in the rest-frame hard band, as a function of the BH mass (and colour coded with the SFR), for the HyLIRGs progenitors with a detectable observed-frame soft[13] F_X^{BH} (i.e. namely the objects located in the hatched region of the histograms in Fig. 5b). We find that HyLIRGs hosting black holes with $M_{BH} \gtrsim 10^7$ M$_\odot$ have X-ray emission dominated by their SMBH activity. In particular, we find that, for about 40 per cent of the these galaxies, the X-ray luminosity due to the nuclear activity is at least one order of magnitude larger than that associated to star formation. Since we are conservatively assuming that the X-ray emission produced by stars is completely unobscured, if L_X^{SFR} were corrected for attenuation,[14] the relative contribution of SMBH activity to the total X-ray emission would be even higher. In conclusions, we find that (i) a significant fraction of HyLIRG progenitors has detectable (obscuration-attenuated) X-ray fluxes produced by accreting BHs in both the observed-frame soft (40 per cent) and hard (38 per cent) bands; (ii) for those objects, the overall $L_X = L_X^{SFR} + L_X^{BH}$ is dominated by L_X^{BH}, making the observed X-ray emission an optimal tracer of SMBH activity. Combining these findings with the predicted spatial density of HyLIRGs (see Section 3.1), we estimate the spatial density of

[13]The observed-frame [0.5-2] keV band traces hard X-ray emission at the redshifts of interest.

[14]GQd model cannot provide information on the spatial distribution of stars, therefore a self-consistent treatment of obscuration of the stellar X-ray emission is very difficult (see Valiante et al. 2016), without coupling detailed hydrodynamical models with radiative transfer simulations accounting for X-ray physics (Smidt et al. 2018; Graziani, Ciardi & Glatzle 2018). On the other hand, a statistical approach is currently impossible due to computational limits.

HyLIRGs with detectable X-ray emission tracing SMBH activity to be $\sim 0.07\,\mathrm{Gpc}^{-3}$.

4 CONCLUSIONS

In the last decade, observations of DSFGs have extended towards $z > 5$. High-z DSFGs are often found to be HyLIRGs ($L_{\rm IR} > 10^{13}\,\mathrm{L}\odot$) with SFRs exceeding $1000\,\mathrm{M}_\odot\,\mathrm{yr}^{-1}$, likely tracing the result of strong dynamical interactions and intense gas accretion events occurring in the densest regions of the early Universe (Walter et al. 2012; Riechers et al. 2017; Pavesi et al. 2018). Recently, Marrone et al. (2018) found an IR-luminous system, SPT0311-58, at $z \sim 7$, composed by a pair of extremely massive and IR-luminous interacting galaxies. Using different proxies to estimate the halo mass hosting the system, they show that SPS0311-58 marks an exceptional peak in the cosmic density field at this early cosmic time and it lies close to the exclusion curve predicted by the current structure formation paradigm. In this work we use GQd model to simulate several independent merger histories of a typical luminous quasar at $z \sim 6$, following the black hole growth and the baryonic evolution (including star formation, metals and dust life cycles, and mechanical feedback) of its ancestors up to $z \sim 10$. We find that

(i) a fraction of progenitor galaxies (about 0.4 objects per single luminous quasar, between $z \sim 6-8$) has HyLIRGs-like IR luminosity of $L_{\rm IR} > 10^{13}\,L_\odot$ (see Fig. 2) and similar characteristics to the system observed by Marrone et al. (2018) (e.g. generally highly massive, extremely star-bursting, and chemically evolved; see Fig. 3);

(ii) the IR-luminous progenitors of $z \sim 6$ quasar host galaxies, reside in the most massive DM haloes, with masses of $M_{\rm DM} \sim 10^{12.5} - 10^{13}\,\mathrm{M}_\odot$ (see Fig. 1). Their far-IR continuum fluxes can be easily observed with ALMA with a modest amount of time, ranging from few seconds in Bands [8, 7, 6] (centred at observed-frame [0.7, 0.95, 1.25] mm, respectively) to about 2 min in Band 4 (2 mm) and 20 min in Band 3 (3 mm).

(iii) the HyLIRGs progenitors of high-z quasar host galaxies have nuclear black holes with masses $10^5\,\mathrm{M}_\odot < M_{\rm BH} < 10^8\,\mathrm{M}_\odot$. The X-ray fluxes associated to the nuclear BH activity could be detectable in the observed-frame soft and hard X-ray bands (they lie above the sensitivity limit of the 7 Ms *Chandra* Deep Field South Survey) for ∼40 per cent of these galaxies, even accounting for obscuration, and dominate over the X-ray emission associated to star formation.

Altogether our results suggest that $z \sim 6$ luminous quasars are, indeed, the signposts of the observed rare high-z overdensities, and that massive-IR luminous galaxies at higher z are their natural ancestors. These findings corroborate models of SMBH–galaxy co-evolution predicting an evolutionary link between IR-luminous galaxies and quasars.

ACKNOWLEDGEMENTS

The authors would like to thank D. Marrone for helpful discussions. The research leading to these results has received funding from the European Research Council under the European Union's Seventh Framework Programme (FP/2007-2013)/ERC Grant Agreement no. 306476. We have benefited from the public available programming language Python, including the numpy, matplotlib, and scipy packages. This research made extensive use of ASTROPY, a community-developed core Python package for Astronomy (Astropy Collaboration et al. 2013), and glueviz, a Python library for multidimensional data exploration (Beaumont, Goodman & Greenfield 2015).

REFERENCES

Alexander D. M., Hickox R. C., 2012, New Astron. Rev., 56, 93
Astropy Collaboration, 2013, A&A, 558, A33
Beaumont C., Goodman A., Greenfield P., 2015, in Taylor A. R., Rosolowsky E., eds, ASP Conf. Ser. Vol. 495, Astronomical Data Analysis Software an Systems XXIV (ADASS XXIV), Astron. Soc. Pac., San Francisco, p. 101
Beelen A., Cox P., Benford D. J., Dowell C. D., Kovács A., Bertoldi F., Omont A., Carilli C. L., 2006, ApJ, 642, 694
Bertoldi F., Carilli C. L., Cox P., Fan X., Strauss M. A., Beelen A., Omont A., Zylka R., 2003, A&A, 406, L55
Bianchi S., Schneider R., 2007, MNRAS, 378, 973
Bischetti M., Maiolino R., Fiore S. C. F., Piconcelli E., Fluetsch A., 2018, preprint (arXiv:1806.00786)
Blain A. W., Smail I., Ivison R. J., Kneib J. P., Frayer D. T., 2002, Phys. Rep., 369, 111
Brightman M. et al. 13, MNRAS, 433, 2485
Bromm V., 2013, Rep. Progr. Phys., 76, 112901
Capak P. L. et al., 2011, Nature, 470, 233
Carlstrom J. E. et al., 2011, PASP, 123, 568
Casey C. M., Narayanan D., Cooray A., 2014, Phys. Rep., 541, 45
Cattaneo A., Bernardi M., 2003, MNRAS, 344, 45
Ceccarelli C., Viti S., Balucani N., Taquet V., 2018, MNRAS, 476, 1371
Chapman S. C., Blain A. W., Smail I., Ivison R. J., 2005, ApJ, 622, 772
Cicone C. et al., 2015, A&A, 574, A14
Coppin K. E. K. et al., 2008, MNRAS, 389, 45
da Cunha E. et al., 2013, ApJ, 766, 13
de Bennassuti M., Schneider R., Valiante R., Salvadori S., 2014, MNRAS, 445, 3039
De Rosa G., Decarli R., Walter F., Fan X., Jiang L., Kurk J., Pasquali A., Rix H. W., 2011, ApJ, 739, 56
Di Matteo T., Springel V., Hernquist L., 2005, Nature, 433, 604
Dunne L., Eales S., Edmunds M., Ivison R., Alexander P., Clements D. L., 2000, MNRAS, 315, 115
Fan L., Knudsen K. K., Fogasy J., Drouart G., 2018, ApJ, 856, 5F
Fan X. et al., 2003, AJ, 125, 1649
Fan X. et al., 2004, AJ, 128, 515
Galliano F. et al., 2011, A&A, 536, A88
Galliano F., Galametz M., Jones A. P., 2018, ARA&A, 56, 673
Ginolfi M., Graziani L., Schneider R., Marassi S., Valiante R., Dell'Agli F., Ventura P., Hunt L. K., 2018, MNRAS, 473, 4538
Graziani L., Ciardi B., Glatzle M., 2018, MNRAS, 479, 4320
Harrison C. M. et al., 2012, MNRAS, 426, 1073
Harrison I., Hotchkiss S., 2013, J. Cosmol. Astropart. Phys., 2013, 022
Hayward C. C., Kereš D., Jonsson P., Narayanan D., Cox T. J., Hernquist L., 2011, ApJ, 743, 159
Hayward C. C., Narayanan D., Kereš D., Jonsson P., Hopkins P. F., Cox T. J., Hernquist L., 2013, MNRAS, 428, 2529
Hopkins P. F., Hernquist L., Cox T. J., Di Matteo T., Robertson B., Springel V., 2006, ApJS, 163, 1
Hopkins P. F., Richards G. T., Hernquist L., 2007, ApJ, 654, 731
Hopkins P. F., Hernquist L., Cox T. J., Kereš D., 2008, ApJS, 175, 356
Hughes D. H. et al., 1998, Nature, 394, 241
Ivison R. J., Papadopoulos P. P., Smail I., Greve T. R., Thomson A. P., Xilouris E. M., Chapman S. C., 2011, MNRAS, 412, 1913
Jiang L. et al., 2016, ApJ, 833, 222
Jones A. P., Köhler M., Ysard N., Bocchio M., Verstraete L., 2017, A&A, 602, A46
Kovács A., Chapman S. C., Dowell C. D., Blain A. W., Ivison R. J., Smail I., Phillips T. G., 2006, ApJ, 650, 592
Lacey C., Cole S., 1993, MNRAS, 262, 627
Lehmer B. D. et al., 2016, ApJ, 825, 7
Luo B. et al., 2017, ApJS, 228, 2

Madau P., Dickinson M., 2014, Annu. Rev. Astron. Astrophys., 52, 415
Magdziarz P., Zdziarski A. A., 1995, MNRAS, 273, 837
Maiolino R. et al., 2005, A&A, 440, L51
Maiolino R. et al., 2012, MNRAS, 425, L66
Marrone D. P. et al., 2018, Nature, 553, 51
Murray S. G., Power C., Robotham A. S. G., 2013, Astron. Comput., 3, 23
Narayanan D. et al., 2015, Nature, 525, 496
Oteo I. et al., 2016, ApJ, 827, 34
Pavesi R. et al., 2018, ApJ, 861, 43
Pezzulli E., Valiante R., Schneider R., 2016, MNRAS, 458, 3047
Pezzulli E., Valiante R., Orofino M. C., Schneider R., Gallerani S., Sbarrato T., 2017, MNRAS, 466, 2131
Richards G. T. et al., 2006, ApJS, 166, 470
Riechers D. A. et al., 2011, ApJ, 733, 11
Riechers D. A. et al., 2013, Nature, 496, 329
Riechers D. A. et al., 2017, ApJ, 850, 1
Robson I., Priddey R. S., Isaak K. G., McMahon R. G., 2004, MNRAS, 351, L29
Romano-Diaz E., Shlosman I., Trenti M., Hoffman Y., 2011, ApJ, 736, 66
Salvadori S., Schneider R., Ferrara A., 2007, MNRAS, 381, 647
Salvadori S., Ferrara A., Schneider R., 2008, MNRAS, 386, 348
Sanders D. B., Soifer B. T., Elias J. H., Madore B. F., Matthews K., Neugebauer G., Scoville N. Z., 1988a, ApJ, 325, 74
Sanders D. B., Soifer B. T., Elias J. H., Neugebauer G., Matthews K., 1988b, ApJ, 328, L35
Sazonov S. Y., Ostriker J. P., Sunyaev R. A., 2004, MNRAS, 347, 144
Silk J., Rees M. J., 1998, A&A, 331, L1
Smail I., Ivison R. J., Blain A. W., 1997, ApJ, 490, L5
Smidt J., Whalen D. J., Johnson J. L., Surace M., Li H., 2018, ApJ, 865, 126
Springel V. et al., 2005, Nature, 435, 629
Strandet M. L. et al., 2016, ApJ, 822, 80
Strandet M. L. et al., 2017, ApJ, 842, L15
Tanaka T., Haiman Z., 2009, ApJ, 696, 1798
Valiante R., Schneider R., Salvadori S., Bianchi S., 2011, MNRAS, 416, 1916
Valiante R., Schneider R., Maiolino R., Salvadori S., Bianchi S., 2012, MNRAS, 427, L60
Valiante R., Schneider R., Salvadori S., Gallerani S., 2014, MNRAS, 444, 2442
Valiante R., Schneider R., Volonteri M., Omukai K., 2016, MNRAS, 457, 3356
Volonteri M., Haardt F., Madau P., 2003, ApJ, 582, 559
Walter F. et al., 2012, Nature, 486, 233
Walter F., Carilli C., Bertoldi F., Menten K., Cox P., Lo K. Y., Fan X., Strauss M. A., 2004, ApJ, 615, L17
Wang R. et al., 2008, ApJ, 687, 848
Weingartner J. C., Draine B. T., 2001, ApJ, 548, 296
Weiß A. et al., 2013, ApJ, 767, 88
Willott C. J. et al., 2010, AJ, 139, 906
Willott C. J., McLure R. J., Jarvis M. J., 2003, ApJ, 587, L15
Yaqoob T., 1997, ApJ, 479, 184
Yue B., Ferrara A., Salvaterra R., Xu Y., Chen X., 2013, MNRAS, 433, 1556
Zappacosta L. et al., 2018, ApJ, 854, 33
Zhukovska S., Dobbs C., Jenkins E. B., Klessen R. S., 2016, ApJ, 831, 147

This paper has been typeset from a TEX/LATEX file prepared by the author.